Bulk termination of the quasicrystalline fivefold surface of $Al_{70}Pd_{21}Mn_9$

Z. Papadopolos* and G. Kasner
Institut für Theoretische Physik, Universität Magdeburg, PSF 4120, D-39016 Magdeburg, Germany

J. Ledieu and E. J. Cox
Surface Science Research Centre, The University of Liverpool, Liverpool L69 3BX, United Kingdom

N. V. Richardson and Q. Chen
Department of Chemistry, University of St. Andrews, Fife, Scotland

R. D. Diehl
Department of Physics, Pennsylvania State University, University Park, Pennsylvania 16802

T. A. Lograsso and A. R. Ross
Ames Laboratory, Iowa State University, Ames, Iowa 50011

R. McGrath
Surface Science Research Centre and Department of Physics, The University of Liverpool, Liverpool L69 3BX, United Kingdom
(Received 25 November 2001; published 18 November 2002)

The structure of the $Al_{70}Pd_{21}Mn_9$ surface has been investigated using high-resolution scanning tunneling microscopy. From two large fivefold terraces on the surface in a short decorated Fibonacci sequence, atomically resolved surface images have been obtained. One of these terraces carries a rare local configuration in the form of a ring. The location of the corresponding sequence of terminations in the bulk model $\mathcal{M}$ of icosahedral *i*-AlPdMn based on the three-dimensional tiling $\mathcal{T}^{*(2F)}$ of an F phase has been estimated using this ring configuration and the requirement from low-energy electron diffraction work of Gierer *et al.* that the average atomic density of the terminations is 0.136 atoms per Å^2. A termination contains two atomic plane layers separated by a vertical distance of 0.48 Å. The position of the bulk terminations is fixed within the layers of Bergman polytopes in the model $\mathcal{M}$: they are 4.08 Å in the direction of the bulk from a surface of the most dense Bergman layers. From the coding windows of the top planes in terminations in $\mathcal{M}$ we conclude that a Penrose (P1) tiling is possible on almost all fivefold terraces. The shortest edge of the tiling P1 is either 4.8 or 7.8 Å. The experimentally derived tiling of the surface with the ring configuration has an edge length of 8.0 $\pm$0.3 Å and hence matches the minimal edge length expected from the model.

DOI: 10.1103/PhysRevB.66.184207 PACS number(s): 61.44.Br, 68.35.Bs, 68.37.Ef, 61.14.Hg

I. INTRODUCTION

More than ten years ago, the discovery that centimeter-sized samples of decagonal *d*-AlCuCo and icosahedral *i*-AlPdMn could be grown opened up the possibility of surface studies of these quasicrystals.[1] Since then, other quasicrystal samples have been grown to similar dimensions. To date, most surface studies have been performed on the fivefold surface of *i*-AlPdMn.[2–14] A consensus has emerged from these studies that this surface, after fairly standard ultrahigh-vacuum (UHV) sputtering and annealing procedures, is itself quasicrystalline. In this work, using a combined experimental and theoretical approach, we show that this surface can be considered to be a termination of the known bulk structure.[15–21]

The dynamical low-energy electron diffraction (LEED) analysis carried out by Gierer *et al.*[13,14] indicated that the fivefold surface of the *i*-AlPdMn quasicrystal retained bulk quasicrystallinity.[13,14] X-ray photoelectron diffraction (XPD) studies are also consistent with a quasicrystalline surface nature.[10–12] Large flat terraces may be produced, and scanning tunneling microscopy (STM) studies have presented similar images of the quasicrystalline surface.[2–5,7–9] Schaub *et al.*[2–5] produced detailed STM images of the terraces that reveal a dense distribution of *dark pentagonal holes* of edge length circa 4.8 Å oriented parallel to each other, together with a more random distribution of bright protrusions. They correlated measurements of structural elements both within the terraces and across steps on the surface.

Later, we demonstrated a correspondence of these measurements with the geometric model $\mathcal{M}$ (Refs. 19–21) for atomic positions of an F phase.[22] The model $\mathcal{M}$ is based on the three-dimensional icosahedral tiling $\mathcal{T}^{*(2F)}$(Ref. 23) decorated essentially by Bergman/Mackay polytopes.[16–18,24] The observed terrace structure of the surface was explained in terms of the layer structure of the bulk model. The dark pentagons observed on the surface corresponded to the Bergman polytopes[25] in the bulk layers. The position of a given type of terrace was matched to a layer characterized by a density of certain Bergman polytopes and their distribution pattern. We assumed that the surface termination respects the integrity of the Bergman polytopes as clusters, at least in the most dense layers, and we supposed that such a layer of Bergman polytopes is exactly below the termination. How-

ever, under these assumptions it was not possible to explain the observed edge length (circa 4.8 Å) of the dark pentagonal holes, as this was bigger by the factor of $\tau=(\sqrt{5}+1)/2$ than the pentagonal surfaces of the Bergman polytope (circa 3 Å).[19]

Later Shen *et al.*, using an autocorrelation analysis, showed that the surface structure is consistent with a bulk structure based on truncated pseudo-Mackay icosahedra[7] and (therefore) Bergman clusters. A fundamental limit of those previous STM studies (Refs. 2–10), was that the resolution of the images, while subnanometer, was not atomic. Therefore direct comparison with bulk models was not straightforward. Additionally, the presence of bright protrusions disrupted any attempted tiling, and so comparison with tiling models was not possible. In a previous paper, we reported an improved sample preparation technique. This led to a more perfect surface devoid of protrusions (Sec. III), and this in turn led to improved resolution in the STM images. The better resolution, together with the structural perfection, allowed us to demonstrate that the surface structure is consistent with a bulk termination,[26] using the bulk model of Boudard *et al.*[15]

In this paper we try to find the position of terminations in the bulk model $\mathcal{M}$ demanding (i) that the terminations be ordered in a decorated Fibonacci sequence (Secs. II A and II C) as in Refs. 19–21 and (ii) that the average density of terminations be 0.136 atoms per Å^2, as determined by Gierer *et al.*[13,14] (Sec. II D). The atomically resolved images of the surface that allow us to map the local patterns of the STM images (Secs. III and IV A) to the local atomic configurations in the terminations in $\mathcal{M}$ (Sec. IV A) also prove our ansatz from Sec. II D which fixes the position of the bulk termination to be 4.08 Å deeper within the layer of Bergman polytopes than we expected in Refs. 19–21. With this new position of the termination, the edge length of the dark pentagonal holes observed by Schaub *et al.* in Refs. 2–5 (and already considered in Ref. 19) is now understood (Sec. IV A). Moreover, we conclude that the termination is highly dense in dark pentagonal holes that we can now interpret as *dissected* Bergman (cB) polytopes (Sec. IV A). For the imaged surface terraces the densities of single atomic planes in corresponding terminations are given and their positions with respect to the Bergman layers are discussed (Sec. IV A).

From the general knowledge of possible tilings and coverings in fivefold planes in the model $\mathcal{M}$ developed in Sec. II B, we analyze in Sec. II D the possibility of the existence of the P1 tiling on model terminations. From the predicted coding windows of the top fivefold q planes in terminations in $\mathcal{M}$ (Sec. IV A) we conclude that the Penrose (P1) tiling is possible on almost all fivefold terraces. In Sec. IV B we superimpose exact patches of the P1 tiling on STM images of two large terraces.

II. THEORETICAL BACKGROUND

A. Geometric model $\mathcal{M}$

A geometric model $\mathcal{M}$ for the atomic positions of *i*-AlPdMn or *i*-AlCuFe (Refs. 17 and 18) has been used to interpret the STM measurements data of Schaub *et al.*[2,4] on the fivefold surfaces of *i*-AlPdMn.[19,20] In the model $\mathcal{M}$, the F-phase[27] (see Ref. 22) three-dimensional tiling $\mathcal{T}^{*(2F)}$(Ref. 23) is decorated by Bergman (and automatically Mackay) polytopes.[17,18] For details on Bergman and Mackay polytopes, see Ref. 16. The geometric model is based on the Katz-Gratias model[24] that is explained by Elser[16] in a three-dimensional ''parallel space'' $\mathbb{E}_{\parallel}$, the space in which the model projected from the D_6 lattice[28] (see Refs. 29 and 22) exists. The atoms of *i*-AlPdMn (Ref. 30) or of *i*-AlCuFe (Ref. 24) can be placed on three translational classes of atomic positions with respect to the D_6 lattice and are denoted by q_{D_6} $(\equiv q)$, b, and a; see Table I in Sec. II C and Ref. 20. These atomic positions in $\mathbb{E}_{\parallel}$ are coded by the corresponding ''windows'' or ''acceptance domains'' in the three-dimensional ''perpendicular space'' $\mathbb{E}_{\perp}$. Note that the six-dimensional D_6 lattice, which models an F phase,[22] acts in the six-dimensional space that is a sum of $\mathbb{E}_{\parallel}$ and $\mathbb{E}_{\perp}$. These windows in $\mathbb{E}_{\perp}$ are denoted by W_q, W_b, and W_a, respectively. The windows of the model $\mathcal{M}$ were constructed in Refs. 17, 18, and 20. The tiling $\mathcal{T}^{*(2F)}$ defines the quasiperiodic structure. More accurately, the model $\mathcal{M}$ is supported by $\tau\mathcal{T}^{*(2F)}$, the tiling $\mathcal{T}^{*(2F)}$scaled by the factor $\tau=(\sqrt{5}+1)/2$. The quasilattice points of $\tau\mathcal{T}^{*(2F)}$are in the class of $q\in D_6$.

All points of the quasilattice which contains the vertices of the tiling $\mathcal{T}^{*(2F)}$ can be embedded in a sequence of planes orthogonal to the fivefold symmetry axis of an icosahedron (''fivefold direction''). The planes orthogonal to the axis are the ''fivefold planes.'' The planes appear in a sequence and have been classified (by particular coding regions in the window $W_{\mathcal{T}^{*2F}}$) into five types, ±1, ±2, ±3, ±4, ±5; see Ref. 19. The planes of types 1–4 are ordered in the Fibonacci sequence with intervals m and l. If the planes of type 5 are included, the sequence of planes forms a ''decorated Fibonacci sequence'' with separations s (short), m (medium), and l (long), where $l=\tau m=\tau^2 s$; see Fig. 13 in Sec. IV A. How is the decorated Fibonacci sequence defined? Let us consider the Fibonacci sequence of intervals $M=l$ and $L=\tau l$. If we rename M by l and ''decorate'' the interval L by two points, such that $L=m\cup s\cup m$, the decorated Fibonacci sequence appears. For the *i*-AlPdMn that has the standard distance parallel to the fivefold direction is ⑤ $=4.56$ Å and is modeled by $\tau\mathcal{T}^{*(2F)}$, $s=[2/(\tau+2)]$ ⑤ $=2.52$ Å, $m=\tau[2/(\tau+2)]$ ⑤ $=4.08$ Å, and $l=\tau^2[2/(\tau+2)]$ ⑤ $=6.60$ Å.

In the planes of type 1 a quasiperiodic tiling $\mathcal{T}^{*(A_4)}$(Ref. 31) appears (Refs. 19 and 32) scaled by a factor τ. In the planes of types 2, 3, and 4, fragments of the same tiling of a plane by golden triangles appear (see Ref. 19, Fig. 7) with the same inflation properties as in the tiling $\mathcal{T}^{*(A_4)}$.[31,32]

In Refs. 19 and 21 the model is compared to the ideal icosahedral monograin under the assumption that the terraces on the surface of the material are like the planes in the bulk, i.e., not reconstructed. We will first assume and then support in this paper. The terraces observed by Schaub *et al.*[2,4] were related to the sequence of the planes of the model $\mathcal{M}$ described above; see also Ref. 19. Whereas Schaub *et al.*, after annealing at $\approx 800\,^{\circ}$C, observed only Fibonacci-

ordered step heights m and l on the surface,[2,4] Shen *et al.*, after annealing at $\approx 630\,^{\circ}\mathrm{C}$, also detected the step height s; see Ref. 7.

In this paper we study the fine structure (local atomic configurations) within the observed terraces and compare it to the geometric model $\mathcal{M}$.[19] Whereas in Ref. 19 we succeeded in relating the sequence of the terracelike fivefold surfaces of Schaub *et al.*[2,4] *to the layers* of the Bergman polytopes in the geometric model $\mathcal{M}$, in this paper, using high-resolution STM images of a fivefold surface we will fix the position of the planes within the layers of Bergman polytopes.

In order to recognize and identify the fine structure of the observed surface, we consider certain tilings in the fivefold planes and a covering with a set of prototiles among which are the pentagons and pentagonal stars.[33] These tilings will be locally derived from the tiling $\mathcal{T}^{*(A_4)}$. The local derivation will be exact to a certain stage and, thereafter, random. The tiling $\mathcal{T}^{*(A_4)}$ scaled by the factor τ defines the quasiperiodic structure of the planes on the surfaces according to the model $\mathcal{M}$ introduced above.[19] The prototiles in the tiling $\mathcal{T}^{*(A_4)}$are golden triangles. The edges of the triangles in the tiling are parallel to the twofold symmetry axes of an icosahedron (''twofold directions'') and are of two lengths ② and τ②. The three-dimensional model $\mathcal{M}$ is supported by the tiling $\tau\mathcal{T}^{*(2F)}$and consequently in the fivefold surfaces by $\tau\mathcal{T}^{*(A_4)}$. Hence the edges are τ② and $\tau^2$②. With the standard value ②$=4.795$ Å in the case of *i*-AlPdMn, τ② $=7.758$ Å and $\tau^2$②$=12.553$ Å.

The structure on the surface observed by STM can be tiled uniquely *only* if the tiling, as an abstract structure, is derivable from the set of quasilattice points and if the rules of the local derivation are defined on relatively small distances with respect to the area of the observed surface.

B. Tilings and coverings with pentagonal prototiles contained in the tiling $\mathcal{T}^{*(A_4)}$

As an intermediate step we locally derive the tiling $\mathcal{T}^{*(z)}$ with pentagon, acute rhombus, and hexagon as prototiles from the quasilattice $\mathcal{T}^{*(A_4)}$, as shown in Fig. 1. The tiling has an inflation factor τ. It is clear that the tiling $\mathcal{T}^{*(z)}$ can be reconstructed from its own quasilattice points. All edges of the prototiles in $\mathcal{T}^{*(z)}$ are of length τ②. In the geometric model $\mathcal{M}$ the prototiles are augmented by a factor τ, so the edge length is $\tau^2$②$=12.553$ Å. All prototiles of $\mathcal{T}^{*(z)}$are the unions of golden triangles of the previous tiling $\mathcal{T}^{*(A_4)}$, as shown in Fig. 1. If we keep that content, the window of the tiling is identical to the window of $\mathcal{T}^{*(A_4)}$ [because none of the vertex (quasilattice) points is omitted]. The coding window of the tiling $\mathcal{T}^{*(z)}$, without the content of golden triangles, is shown in Fig. 2. Small fractions of the tiling $\mathcal{T}^{*(z)}$ have been observed in the fivefold surfaces of decagonal (d)-AlCuCo.[34]

From the intermediate tiling $\mathcal{T}^{*(z)}$ we can locally derive a *covering* of the tiling $\mathcal{T}^{*(A_4)}$. This covering is by two cells in the shape of pentagons, the smaller one $D_{\parallel}^{a}$ of edge length ② and the bigger one $D_{\parallel}^{b}$ of edge length τ②, as shown in Fig. 3(a). Let us denote this covering of the tiling $\mathcal{T}^{*(A_4)}$ by

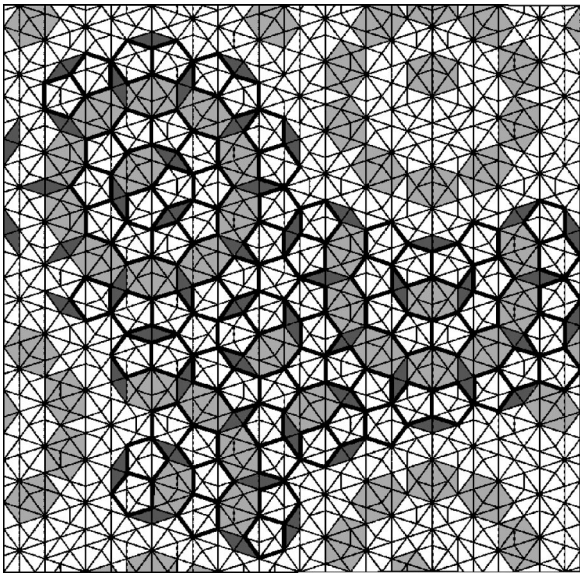

FIG. 1. The tiling $\mathcal{T}^{*(z)}$ of the plane with the acute rhombus, pentagon, and hexagon as the prototiles. The tiles are marked by thick lines and different gray shadows. The tiling $\mathcal{T}^{*(A_4)}$, from which $\mathcal{T}^{*(z)}$is locally derived, is shown in the background using thin lines.

$\mathcal{C}^{s}_{\mathcal{T}^{*(A_4)}}$. Each acute rhombus from $\mathcal{T}^{*(z)}$ is transformed into a pair of pentagons of edge length ②[shown in the left-hand side of Fig. 3(a)], and each hexagon is transformed into a pair of overlapping pentagons of edge length τ② [right-hand side of Fig. 3(a)]. The remainder of the tiling $\mathcal{T}^{*(A_4)}$should be covered by pentagons of edge length τ② as in the tiling $\mathcal{T}^{*(z)}$; see Fig. 1. The above-defined covering $\mathcal{C}^{s}_{\mathcal{T}^{*(A_4)}}$of the tiling $\mathcal{T}^{*(A_4)}$ is a subcovering of the covering of Kramer.[35,36] Kramer also covers the tiling $\mathcal{T}^{*(A_4)}$ by two pentagons of the same size as above. These cells are projected Delone cells D^a and D^b of the lattice A_4 in $\mathbb{E}_{\parallel}$. In $\mathbb{E}_{\parallel}$ they are denoted by $D_{\parallel}^{a}$ and $D_{\parallel}^{b}$, respectively. Let us denote Kramer's covering by the symbol $\mathcal{C}^{k}_{\mathcal{T}^{*(A_4)}}$. The set of pentagons in $\mathcal{C}^{s}_{\mathcal{T}^{*(A_4)}}$of edge length τ② is identical to the set of $D_{\parallel}^{b}$'s in $\mathcal{C}^{k}_{\mathcal{T}^{*(A_4)}}$. The set of pentagons in $\mathcal{C}^{s}_{\mathcal{T}^{*(A_4)}}$of edge length ②, derived from

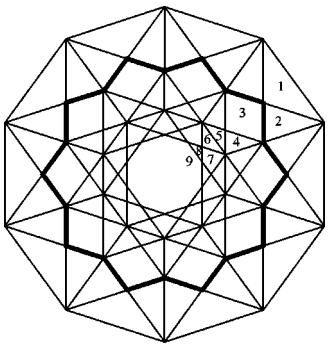

FIG. 2. The coding window of the tiling $\mathcal{T}^{*(z)}$, without the content of golden triangles, is inscribed in the decagon by thick lines, which is the coding window of the tiling $\mathcal{T}^{*(A_4)}$. The codings of the nine types of vertex configurations in the tiling $\mathcal{T}^{*(A_4)}$are marked by the numbers 1–9.

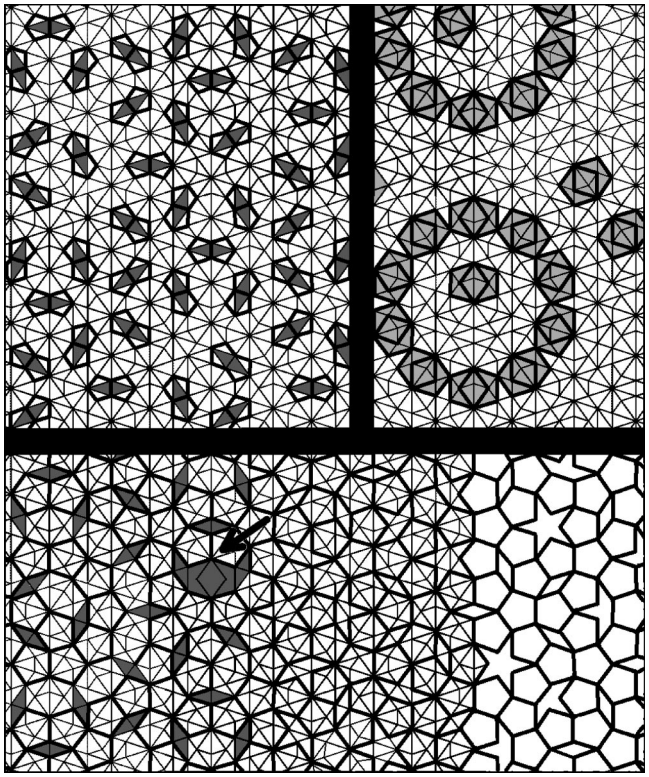

FIG. 3. (a) The derivation $\mathcal{T}^{*(z)} \rightarrow \mathcal{C}^{s}_{\mathcal{T}^{*(A_4)}}$is in the *top* part of the figure. (b) $\mathcal{T}^{*(z)} \rightarrow \mathcal{T}^{*(p1)_r}$ is in the *bottom* part of the figure.

the acute rhombuses, is a *subset* of the set of all $D^a_{\parallel}$'s in $\mathcal{C}^{k}_{\mathcal{T}^{*(A_4)}}$, and *therefore* the covering $\mathcal{C}^{s}_{\mathcal{T}^{*(A_4)}}$of $\mathcal{T}^{*(A_4)}$ is a *subcovering* of the covering $\mathcal{C}^{k}_{\mathcal{T}^{*(A_4)}}$.[35,36] Whereas the thickness of the covering of $\mathcal{C}^{k}_{\mathcal{T}^{*(A_4)}}$is $C^k = 3 - \tau \approx 1.382$, the thickness of the covering of the subcovering $\mathcal{C}^{s}_{\mathcal{T}^{*(A_4)}}$is $C^s = 2\tau - 2 \approx 1.236 < 1.382$. (For an explanation of the thickness of the covering see Ref. 37. As a reference: the thickness of the covering of a space by a tiling always equals 1.) In the subcovering $\mathcal{C}^{s}_{\mathcal{T}^{*(A_4)}}$only the single and double decking (covering) (Ref. 37) of the tiles by the covering clusters are present. The triple decking, which exists in the covering $\mathcal{C}^{k}_{\mathcal{T}^{*(A_4)}}$, is excluded[37] in $\mathcal{C}^{s}_{\mathcal{T}^{*(A_4)}}$. The window of the subcovering $\mathcal{C}^{s}_{\mathcal{T}^{*(A_4)}}$of $\mathcal{T}^{*(A_4)}$ by two pentagons *without* the content of golden triangles is presented in Fig. 4.

From the tiling $\mathcal{T}^{*(z)}$ let us keep all acute rhombuses and replace each hexagon by two overlapping pentagons (as in the subcovering $\mathcal{C}^{s}_{\mathcal{T}^{*(A_4)}}$). This is an exact local derivation, shown in the left-hand side of Fig. 3(b). At this stage we *randomly* choose one of the pentagons from each overlapping pair, and the rest of each hexagon unites with the neighboring acute rhombus. In this way, either a crown or a pentagonal star appears to replace the rhombus, and we obtain a partly random tiling $\mathcal{T}^{*(p1)_r}$; see the right-hand side of Fig. 3(b). The ideal class of tilings (P1) with the inflation factor τ are described in Refs. 38 and 39. In Fig. 5(a), the window that exactly defines the quasilattice of the tiling $\mathcal{T}^{*(p1)}$ is inscribed in the window of the tiling $\mathcal{T}^{*(A_4)}$.

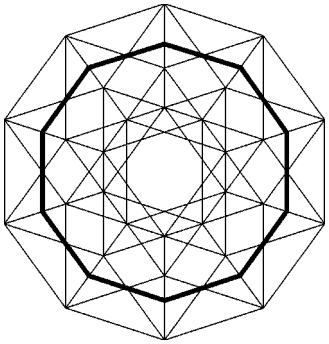

FIG. 4. The window of the covering $\mathcal{C}^{s}_{\mathcal{T}^{*(A_4)}}$without the content of golden triangles, inscribed by the thick lines in the window of the tiling $\mathcal{T}^{*(A_4)}$.

There is another tiling of a plane by pentagonal stars, pentagons and obtuse rhombuses introduced by Niizeki.[39] Let us call it the Niizeki star tiling and denote it by $\mathcal{T}^{*(n)}$. The inflation factor of this tiling is also τ. In Fig. 6 we derive this tiling from the tiling $\mathcal{T}^{*(z)}$. In Fig. 6(a) (top part of Fig. 6) on the left-hand side, from the set of all stars, only the locally derivable stars are presented. The locally derivable star appears wherever there exists an acute rhombus neighboring one or two hexagons, each by an edge. Between these stars, there appear obtuse rhombuses. In Fig. 6(a) on the right-hand side the white spaces around the isolated acute rhombuses are framed by thick lines. Inside these patches, there appear pairs of overlapping stars, inscribed in one single place in the figure and marked by an arrow. Their overlap is exactly the acute rhombus. Up to the choice of one star from each pair of overlapping stars, the local derivation of the tiling is exact. The exact tiling of the plane by the stars, obtuse rhombuses, and pentagons, $\mathcal{T}^{*(n)}$, is uniquely determined by its window inscribed in the window of $\mathcal{T}^{*(A_4)}$; see Fig. 5(b). It is the window of the Niizeki tiling. We *randomly* choose a star from each overlapping pair of stars indicated in the bottom part of Fig. 6 and obtain a partly random tiling $\mathcal{T}^{*(n_r)}$. The only edge length that appears in the tiling is τ②(in the geometric model $\mathcal{M}$, it is $\tau^2$② $= 12.553$ Å). It is also the tiling that could be, eventually seen and reconstructed from the STM images of the surfaces

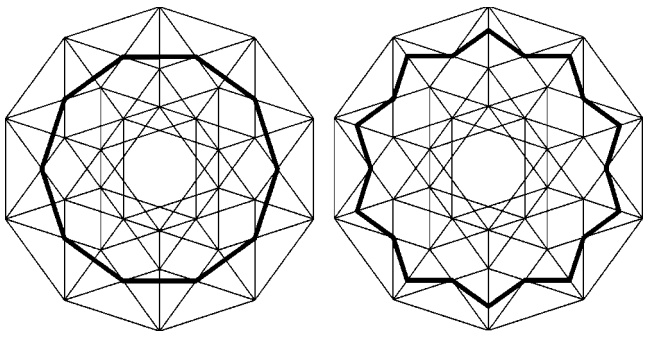

FIG. 5. (a) The window of $\mathcal{T}^{*(p1)}$ is inscribed in the window of $\mathcal{T}^{*(A_4)}$ by thick lines. (b) The exact tiling of the plane by the stars, obtuse rhombuses, and pentagons, $\mathcal{T}^{*(n)}$, is uniquely determined by its window inscribed by thick lines in the window of $\mathcal{T}^{*(A_4)}$. It is the window that codes the Niizeki tiling $\mathcal{T}^{*(n)}$.

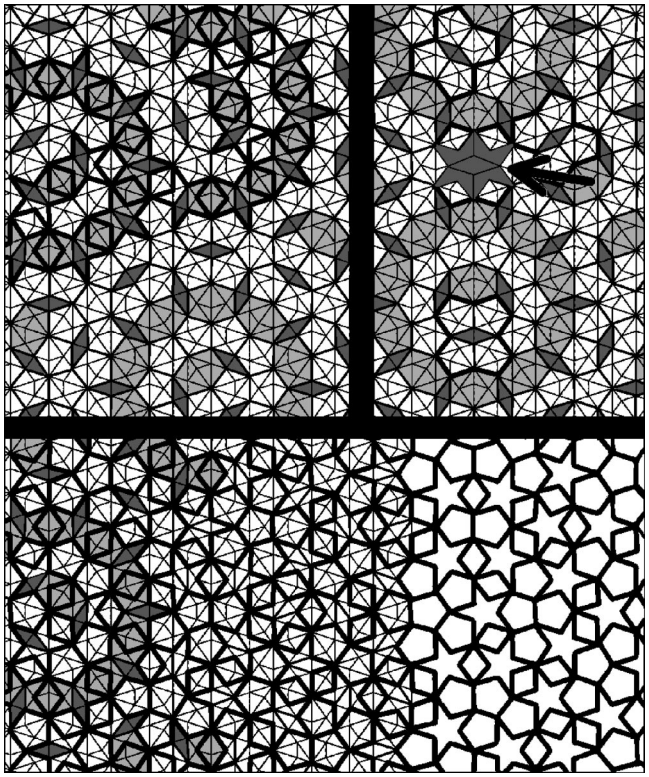

FIG. 6. Local derivation: $\mathcal{T}^{*(z)} \rightarrow \mathcal{T}^{*(n_r)}$. In the text, the top part of the figure is referred to as (a) and the bottom part as (b).

orthogonal to the fivefold direction in *i*-AlPdMn and *i*-AlCuFe and in a decagonal phase.

Both exact tilings $\mathcal{T}^{*(p1)}$ and $\mathcal{T}^{*(n)}$can be locally derived from their respective quasilattice points. In the reconstruction of tilings $\mathcal{T}^{*(p1)}$ and $\mathcal{T}^{*(n)}$ from the respective quasilattices there appear (i) pairs of pentagonal sets of points centered in each other and mutually rotated by $2\pi/10$. The set of points of the smaller size (the smallest pentagonal set in the tiling) is on the neighboring distances ②, the bigger, on neighboring distances $\tau^2$②. Each pair leads to the pentagonal star. (ii) The isolated pentagonal sets with neighboring distances τ② are to be connected in pentagons. In order to reconstruct the tiling $\mathcal{T}^{*(p1)}$, it is enough to draw the pentagons from the isolated fivetuples of fivefold symmetrically ordered points. In order to reconstruct the tiling $\mathcal{T}^{*(n)}$one draws the stars from the pairs of pentagonal sets defined above. One can show that in an abstract sense the tilings $\mathcal{T}^{*(p1)}$ and $\mathcal{T}^{*(n)}$can be mapped one to one to each other.[37] If we consider an experimental atomically resolved fivefold surface and tile the observed surface, we first have to identify the surface by a plane in the model which we will call an $\mathcal{M}$ plane. Then we determine the coding window of the plane in $\mathbb{E}_\perp$, the $\mathcal{M}$-plane window, and we place the biggest possible window of an exact tilings $\mathcal{T}^{*(p1)}$ or $\mathcal{T}^{*(n)}$in the $\mathcal{M}$-plane window; see Figs. 7 and 12, below. Following these arguments, we will determine the edge length of a possible tiling of an observed surface by the prototiles of the tiling P1 in Sec. IV.

TABLE I. The condition for atomic positions $x = \frac{1}{2}(n_1, \ldots, n_6)$ to be in a fivefold plane in $\mathbb{E}_\parallel$ or $\mathbb{E}_\perp$ is a class function. The symbols *e* and *o* stand for even and odd integers, respectively. The symbol $n_\parallel^5/n_\perp^5$ is a unit normal to the fivefold plane in $\mathbb{E}_\parallel/\mathbb{E}_\perp$ space, respectively. $x_\parallel \in \mathbb{E}_\parallel$ and $x_\perp \in \mathbb{E}_\perp$, where *x* is the point in six-dimensional space, $\mathbb{E}_\parallel + \mathbb{E}_\perp$. The scalar product is given in the units $[\kappa]$, $\kappa = 1/[\sqrt{2}(\tau+2)]$.

Class criterion	Class	$n_\parallel^5 \cdot x_\parallel[\kappa]$	$n_\perp^5 \cdot x_\perp[\kappa]$
$\frac{1}{2}(e_1, \ldots, e_6)$; $\frac{1}{2}\Sigma_i e_i =$ even	q_{D_6}	$e+e\tau$	$e+e\tau$
$\frac{1}{2}(e_1, \ldots, e_6)$; $\frac{1}{2}\Sigma_i e_i =$ odd	*b*	$e+o\tau$	$e+o\tau$
$\frac{1}{2}(o_1, \ldots, o_6)$; $\frac{1}{2}\Sigma_i o_i =$ odd	*a*	$o+o\tau$	$o+e\tau$
$\frac{1}{2}(o_1, \ldots, o_6)$; $\frac{1}{2}\Sigma_i o_i =$ even	*c*	$o+e\tau$	$o+o\tau$

C. Atomic positions in fivefold planes of the geometric model $\mathcal{M}$

In Sec. II B we have derived the tilings $\mathcal{T}^{*(z)}$, $\mathcal{T}^{*(p1)}$, and $\mathcal{T}^{*(n)}$ either from the ideal tiling $\mathcal{T}^{*(A_4)}$or from their own corresponding quasilattices. We have been considering exclusively these points $q \in D_6$ which belong to the underlying tiling of the model, $\tau\mathcal{T}^{*(A_4)}$. Consequently the edge lengths in both locally derived tilings, $\mathcal{T}^{*(p1)_r}$ and $\mathcal{T}^{*(n_r)}$, were of length $\tau^2$②$=12.553$ Å. If we also take into account the decoration of the tiling by Bergman/Mackay polytopes, the window of the quasilattice points of type $q \in D_6$, $W_{q_{D_6}}$, becomes the polytope derived in Refs. 17, 18, and 20.

In order to study the fivefold planes of the model $\mathcal{M}$, we present two important general facts that we implicitly use in all our considerations.

(i) The reciprocal lattice of the root lattice D_6 we denote by D_6^{rec}. The lattice D_6^{rec} is also known as the weight lattice D_6^w. If one icosahedrally projects D_6^{rec} to the parallel space, $\mathbb{E}_\parallel/(\mathbb{E}_\perp)$, an icosahedral $\mathbb{Z}(\tau)$module appears.[40,41] The module points in a plane of a three-dimensional (icosahedral) $\mathbb{Z}(\tau)$module in $\mathbb{E}_\parallel$, under the * - map,[41] i.e., $\tau \rightarrow -1/\tau$, are mapped in $\mathbb{E}_\perp$ onto a plane too. The section of this plane in $\mathbb{E}_\perp$ through the three-dimensional window (acceptance region of the three-dimensional quasilattice) defines a two-dimensional window of the quasilattice in a corresponding plane in $\mathbb{E}_\parallel$. The analogous statement holds true for the lines. These are the general properties of a $\mathbb{Z}(\lambda)$ module with quadratic irrationality λ. In our considerations $\lambda = \tau = (\sqrt{5}+1)/2$. The above statement is valid for the modules with symmetries such as icosahedral, fivefold, tenfold, eightfold, and twelvefold.

(ii) Let us consider the four translational classes with respect to the root lattice D_6 of six-dimensional points $\frac{1}{2}(n_1, \ldots, n_6) \in D_6^w$, where n_i are integers. The condition for an atomic position $x = \frac{1}{2}(n_1, \ldots, n_6)$ to be in a fivefold plane in $\mathbb{E}_\parallel$ or $\mathbb{E}_\perp$ is a class function presented in Table I. Hence, the atomic positions in a fivefold plane of a D_6^w-icosahedrally projected $\mathbb{Z}(\tau)$module belong to the *single* class, q_{D_6} $(\equiv q)$, *b*, *a*, or *c*.

Using the facts (i) and (ii), in the geometric model $\mathcal{M}$ we code each fivefold plane containing a class of atomic posi-

tions in $\mathbb{E}_\parallel$ by the fivefold dissection in $\mathbb{E}_\perp$ of the *single* window W_q, W_b, or W_a, corresponding to that class.

D. Densities of fivefold planes and terminations of fivefold surfaces in the geometric model $\mathcal{M}$

In the work of Gierer *et al.*[14] an average density of ''terminations'' of fivefold surfaces has been determined to be $\rho_{q+b}=\rho_q+\rho_b=0.136$ atoms per Å^2. By the density of the termination the authors mean the sum of the densities of two atomic planes on a surface separated by a vertical distance of 0.48 Å, and consequently each ''termination'' corresponds to a pair of planes separated by this distance. Let us suppose that the surface (top) planes are of type *q*; then the planes 0.48 Å below, in the geometric model $\mathcal{M}$, are of type *b*. Let us calculate $\rho_{q+b}(z_\parallel)$ in the model, where $z_\parallel$ is along a fivefold axis orthogonal to terraces on the surface, and let us plot this value along the corresponding $z_\perp$, $\rho_{q+b}(z_\perp)$. The result is shown in Fig. 7.

The function $\rho_{q+b}(z_\perp)$ has a clear (almost flat) plateau. The appearance of the plateau is due to the polytopal shape of the coding windows W_q and W_b in the geometric model $\mathcal{M}$.[17,18,20] In particular the window W_q, which defines the surface (top) plane in a termination, differs strongly from the spherical shape. The plateau of the function $\rho_{q+b}(z_\perp)$ simultaneously contains the maxima of the function and has a value that approximately equals the average density of terminations determined by Gierer *et al.*,[14] which is 0.136 atoms per Å^2. It is easy to conclude that all terminations on terraces must have equal densities. Consequently an interval on $z_\perp$ under the plateau (the ''carrier'' of the plateau) *codes* the terminations and indicates the *new* coding of surface *q* planes to be shifted from the *old* value that we expected in Refs. 19–21. In those papers[19–21] we supposed that a *single*-surface *q* plane has to have the highest density. In accordance with this ansatz, at least some of the dense layers of Bergman polytopes were below the surfaces. But the dark pentagons observed by Schaub *et al.*,[4] which we put in correspondence with the Bergman polytopes in the layer below the surface, were bigger by a factor of τ than the faces of Bergman polytopes.[19] Let us shift the surfaces of terraces by 4.08 Å in the direction of the bulk (-4.08 Å along $z_\parallel$) in ''parallel'' (observable) space, such that the *q* plane on a terrace dissects the Bergman polytopes of the layer and the section of each Bergman polytope is a pentagon of edge length 4.8 Å, approximately the size of the dark pentagons observed by Schaub *et al.*[4] This shift in $\mathbb{E}_\parallel$ corresponds to the shift by $[2\tau/(\tau+2)]$⑤ along $z_\perp$ in orthogonal space. Indeed, the coding interval of *q* planes that forces the planes on the surface to appear in a Fibonacci sequence (or in a decorated Fibonacci sequence) is placed under the plateau of the function $\rho_{q+b}(z_\perp)$ by this shift; see Fig. 7. We suppose that the terracelike fivefold terminations do appear in a Fibonacci (or decorated Fibonacci) sequence such that the top *q* planes in terminations need not be the most dense among the *q* planes, but the above-defined ''terminations,'' the pairs of planes on a surface, have the highest densities among all such pairs of *q* and *b* planes in the geometric model $\mathcal{M}$. We check our hypothesis (ansatz) on two large terraces in Sec. IV.

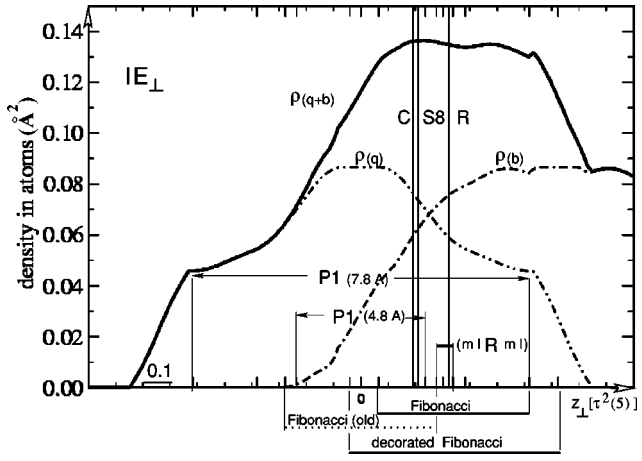

FIG. 7. Density ρ_{q+b} of the pairs of fivefold planes in the bulk model $\mathcal{M}$: a *q* plane and a *b* plane, 0.48 Å *below* the *q* plane. ρ_{q+b} as a function of $z_\perp$ in units of τ^2 ⑤. The image of *z* axes in $\mathbb{E}_\perp$, $z_\perp$, is chosen such that $z_\parallel$ points into the opposite direction of the bulk. $\rho_q(z_\perp)$ is the density of a *q* plane, and $\rho_b(z_\perp)$ is the density of a *b* plane shifted by $c_\perp^{q\to b}=[\tau^4/(\tau+2)]$⑤, $\rho_q(z_\perp)+\rho_b(z_\perp)=\rho_{q+b}(z_\perp)$. In the figure the *old* and *new* coding regions of the (decorated) Fibonacci sequence of planes that represent the surface terraces in $\mathcal{M}$ are marked. In the new region, the representative plane of the biggest clear terrace of Schaub *et al.* (Ref. 4) is marked by S8 on a *new* position. The condition for appearance of the ring plane in a sequence $ml(R)ml$ is determined and a representative of a ring plane (*R*) together with a representative of the following clear plane (*C*) are marked. Finally the region of existence for P1 tilings on a *q* plane is denoted and particular minimal edges are attached to their coding regions; see Sec. IV.

III. FIVEFOLD SURFACES IMAGED BY STM: SURFACE PREPARATION AND STM RESOLUTION

In this section we describe the surface preparation we have developed to obtain large flat terraces and low surface corrugation in STM experiments. We contrast STM results using our optimum preparation with results previously published by us and other groups.[2,7,8]

Figure 8 shows data from the surface of *i*-Al-Pd-Mn after the two different preparation procedures. In each case the quasicrystal samples were grown at Ames Laboratory using the Bridgman method.[42,43] After being cut perpendicular to their fivefold symmetry axes in air, the sample surfaces were prepared[26] by polishing. For the first preparation, preparation I, the sample was polished using 6 and 1 μm diamond paste for 1 h. In-vacuum preparation consisted of a few cycles of argon ion sputtering at 1 keV energy and a normal incidence angle followed by annealing for periods of about 1 h at 970 K. The results are shown in Figs. 8(a) and 8(c). For the second preparation, preparation II, a further polish using 0.25 μm diamond paste was used. The surface was prepared in-vacuum by several cycles of sputtering with 0.5 keV Ar ions, with a sputtering angle of 20°–30° relative to the surface parallel, followed by annealing to 970 K for 2 h (in total 12 h of annealing). Figures 8(b) and 8(d) show the results.

When large-scale scans are compared [Figs. 8(a) and

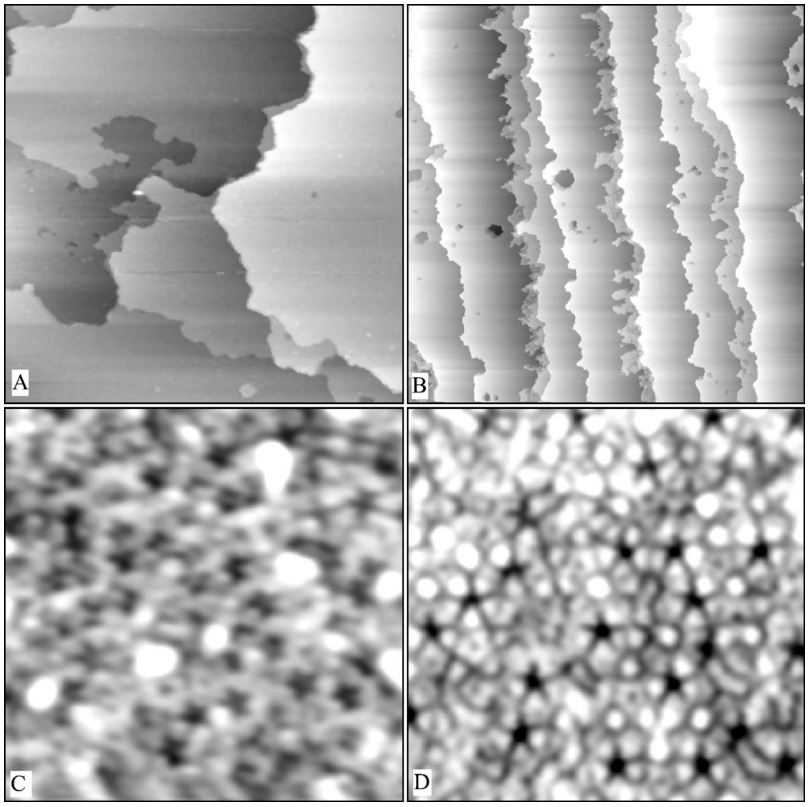

FIG. 8. (a) 1500 Å×1500 Å STM image showing atomically flat terraces from a surface prepared using preparation I. (b) 17 500 Å ×17 500 Å STM image showing atomically flat terraces from a surface prepared using preparation II. (c) 100 Å×100 Å STM image of a flat terrace that we call the ''clear,'' *C* terrace from a surface prepared using preparation I (bias voltage 2.29 V, tip current 0.59 nA). (d) 100 Å×100 Å high-resolution STM image of the same *C* terrace obtained on the fivefold surface using preparation II ($V=1$ V, $I=0.3$ nA).

8(b)], it is evident that larger terraces are obtained using preparation II. For preparation I, the largest terraces are of the order of 1200 Å in magnitude. For preparation II terraces of width 4000 Å and length of micron size were obtained. Further differences between the results of the preparation techniques are observed when scans of smaller area are compared. Figures 8(c) and 8(d) show 100 Å×100 Å areas of each surface. Clearly the surface in Fig. 8(c) is not as well resolved as that in Fig. 8(d); the bright spots in Fig. 8(c) correspond to protrusions of height up to 2.0 Å, while dark spots are associated with holes of depth estimated to be at least 1.5 Å. This STM image is comparable to those in the work of Schaub *et al.*[2–5] This can be contrasted with the surface shown in Fig. 8(d) where there are no large protrusions and the surface corrugation within the terraces is <1 Å. Because the STM tip can scan the surface more

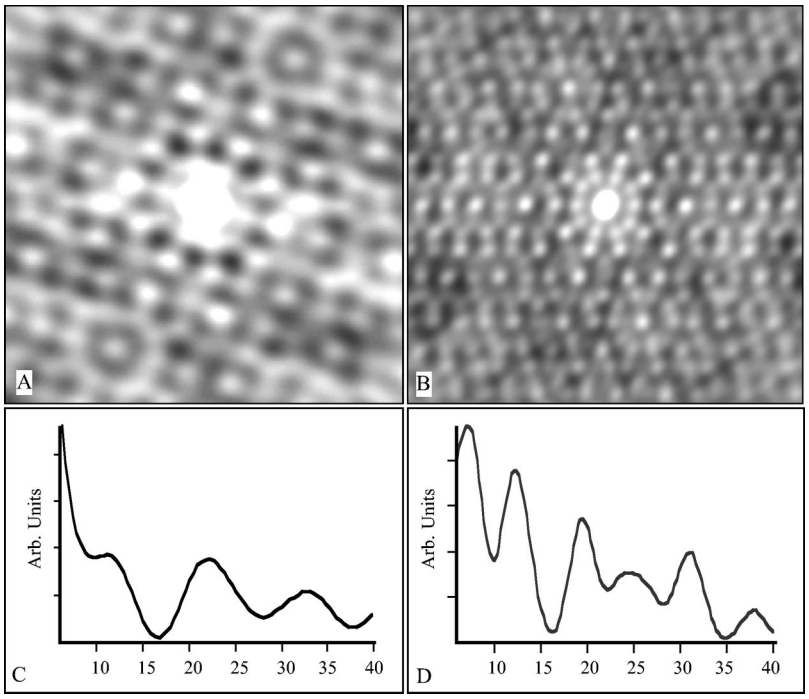

FIG. 9. (a) 100 Å×100 Å lateral autocorrelation function of the STM image of Fig. 8(c). (b) 100 Å×100 Å lateral autocorrelation function of the STM image of Fig. 8(d). (c) Radial distribution function calculated from the autocorrelation pattern of (a). (d) Radial distribution function calculated from the autocorrelation pattern of (b).

closely, features on the surface are better resolved. The features in this image have dimensions typical of atomic sizes (2–3 Å). Larger features (4–6 Å) are also evident and probably represent groups of a few atoms. The LEED patterns from each of these surfaces are qualitatively identical, but the range of electron beam energies over which the LEED patterns are obtained is much larger (10–300 eV) using preparation II than for preparation I (40–180 eV). The LEED patterns have very sharp diffraction spots, a low background, and show fivefold symmetry.

The resolution can be put on a semiquantitative basis by calculating the two-dimensional lateral autocorrelation functions of the images of Figs. 8(c) and 8(d). These are shown in Figs. 9(a) and 9(b), respectively. While the symmetry of both autocorrelation patterns is similar, the pattern of Fig. 9(b) is considerably clearer and the correlation maxima extend to longer distances, indicating a higher degree of quasiperiodic order.

For a more quantitative comparison a radial distribution function (RDF) has been calculated in both cases. The procedure consists of dividing the 360° around the center of the autocorrelation function in increments. Along each line corresponding to each increment, the distances from the center to the maxima are measured. All measurements are then averaged and plotted as histograms [Figs. 9(c) and 9(d)]. It can be seen that there is considerably more structure in the RDF in Fig. 9(d) than in that of Fig. 9(c).

In summary, surfaces prepared using preparation II have a much lower surface corrugation and lead to much better resolved STM data than those previously obtained using preparation I. The main differences in these procedures are the sputtering energy and incidence angle (suggesting that minimizing surface damage while removing contaminants is of importance) and the long anneal times at high temperatures which probably serve to restore the surface composition to that of the bulk quasicrystal. We interpret the protrusions as due to material on the surface which has not yet diffused to the step edges. A similar observation was recently made to explain the origin of such protrusions on *d*-Al-Ni-Co surfaces.[44]

IV. REPRESENTATIONS OF SURFACES ON TERRACES IN THE GEOMETRIC MODEL $\mathcal{M}$: TILING ANALYSIS OF STM IMAGES

A. Fivefold terraces mapped to the terminations in $\mathcal{M}$

In Sec. II D we suggested new positions of fivefold terminations in the geometric model $\mathcal{M}$. In this section we search for the terminations in the geometric model $\mathcal{M}$ on these *new* positions that fit to atomically resolved pictures of fivefold surfaces on particular terraces imaged by STM. In a sequence of fivefold terraces we observe a large terrace that contains a rare local configuration that we call the ''ring'' (R). This configuration helps us to *orient* in the bulk model $\mathcal{M}$, i.e., to fix the position of the R terrace with respect to the fivefold z axes. Near the R terrace we observe the *clearest* terrace that we denote by ''C.'' A fragment of the C terrace is shown in Fig. 8(d).

On the C terrace local configurations of the fivefold depressions in the shape of dark stars (dS) are observed. The strongly shining pentagonal local configurations in the form of the white flower (wF) and the white star pointing upwards (wSu), both parallel to the dS and in the same direction, make a white picture on a dark background; see Fig. 10(a).

In contrast to the C terrace the R terrace is not continuously (globally) clear; i.e., the STM images of the R terrace taken on different places lead to different RDF's. Nevertheless, we observe some local configurations on the R terrace that are clear; see Fig. 11(a). We find the white flower (wF)

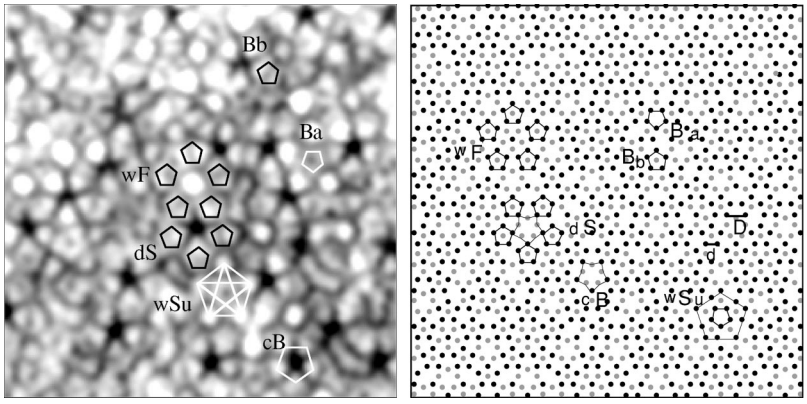

FIG. 10. (a) 100Å×100 Å high-resolution STM image of the C terrace on a fivefold surface. On the C terrace frequently repeated local configurations such as a dark star (dS), a white flower (wF), and a white star pointing upwards (wSu) parallel to the dS are marked. The Bergman polytope below the terrace (Bb), above the terrace (Ba), and the Bergman polytope dissected by the terrace (cB) are also marked. For the scale the wSu is framed by a pentagon of edge length τD, $D \approx 4.8$ Å. (b) The C terrace from (a) corresponds to the C termination in $\mathcal{M}$. Black points are atomic positions in the q-1024 plane in $\mathcal{M}$ (No. 175 in Fig. 13) which is on the surface, grey points are in the b-1025 plane, 0.48 Å below the q-1024 plane. The local atomic configurations that may present the dS, wF, and wSu are marked. The main constituents of these configurations are the top surface of the Bergman polytopes that are in the layer below the surface (Bb), the bottom surface of the Bergman polytopes that are in the layer above the surface (Ba), and the pentagonal section of the Bergman polytopes from the layer that is dissected by the surface (cB). Scale: $D = \tau d = 4.8$ Å. From the center of cB the next atomic position in the bulk is 2.04 Å below the surface.

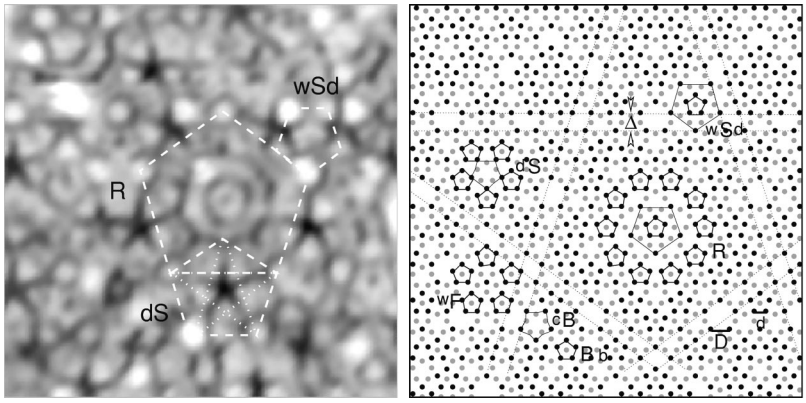

FIG. 11. (a) 75 Å×75 Å STM image of the *R* terrace. The local configurations ring (*R*), dark star (dS), and white star pointing downwards (wSd) are framed by three pentagons of edge lengths $\tau^3 D$, $\tau^2 D$, and τD, respectively, where $D \approx 4.8$ Å. On a bigger STM image of the *R* termination a full white flower (wF) can be seen also. (b) The *R* terrace from (a) corresponds to the *R* termination in $\mathcal{M}$. Black points are atomic positions in *q*-1037 plane in $\mathcal{M}$ (No. 178 in Fig. 13) which is on the surface; gray points are in *b*-1038 plane, 0.48 Å below the *q*-1037 plane. The local configurations of atomic positions that may represent the dark star (dS), the white flower (wF), and the white star (wSd) antiparallel to the dark star (dS) are marked. Scale: $D = \tau d = 4.8$ Å. In the center of the dark star the nearest atomic position is 2.04 Å below the surface. In the *q*-1037 plane there are empty "streets," $\Delta = 4.56$ Å broad.

and the dark star (dS) identical to those on the *C* terrace [see Fig. 10(a)], but we also see a characteristic "ring" configuration (*R*) that is present on none of the other observed terraces. The terrace is therefore denoted the *R* terrace. In the *R* terrace there is also a configuration which we call the white star pointing downwards (wSd); it is rotated 180° with respect to the wSu that we observe on the *C* terrace.

As we stated the areas of both *R* and *C* terrace are large and they appear in a local upward sequence of steps $ml(R)ml(C)$, where $m \approx 4.08$ Å and $l \approx \tau m$. On the *q* planes of the geometric model $\mathcal{M}$ we find a rare atomic configuration that may represent a local ring configuration on the STM image of the *R* terrace; compare Figs. 11(a) and 11(b). We determine the coding of the ring configuration (*R*) in $\mathbb{E}_\perp$ and demand that the *q* plane containing the ring configuration be found in an upward sequence of the *q* planes $ml(R)ml(C)$ on the new positions (shifted by 4.08 Å; see Sec. II D), and *both R* and *C* planes are to be among the planes from the decorated Fibonacci sequence. From these conditions we find the coding area in $\mathbb{E}_\perp$ along $z_\perp$ of the *R* plane to be in the interval $z_\perp \in (0.198, 0.337)[\tau^2 ⑤]$ marked in Fig. 7. In a patch of the geometric model $\mathcal{M}$ that spreads along $z_\parallel$ axes in an interval of 1195 Å we find only 15 representatives of the *R* plane that fulfill all conditions mentioned above. We choose the *q*-1037 plane (No. 178 in Fig. 13); the plane that is coded in $\mathbb{E}_\perp$ by $z_\perp = 0.323\tau^2 ⑤$ (see Fig. 7). The corresponding *C* plane is then *q*-1024 (No. 175 in Fig. 13) coded by $z_\perp = 0.192\tau^2 ⑤$(see Fig. 7). In Fig. 12 the coding windows of the *R* and the *C* planes are shown. This pair of *R* and *C* planes (one of 15 pairs in the model patch) are taken not far from the estimated model plane S8 for Schaub's terrace No. 8^4 on a new position *q*-1128 (No. 193 in Fig. 13) coded by $z_\perp = 0.211\tau^2 ⑤$ (see Fig. 7).

As we have stated, in contrast to the *R* terrace, the *C* terrace is uniformly clear and it has a unique RDF. Figure 14 (top) corresponds to the RDF calculated from the high-resolution STM image of Fig. 8(d) [identical to the RDF shown in Fig. 9(d)]. Maxima are found at 7.3, 12.1, 19.4, 24.2, 31.1, and 38.0 Å (± 0.3 Å). The radial distribution function calculated from the *C* plane *q*-1024 (No. 175) of the geometric model $\mathcal{M}$ [shown in Fig. 14 (bottom)] is very similar, the main differences being the presence of a double peak at 15 Å and some extra structure at higher distances. The correspondence with the largest intensity peaks is, however, very good.

To the *C* and *R* planes of type *q*, there correspond *C* and *R* terminations, which are pairs of *q* and *b* planes at the surface separated by a vertical distance of 0.48 Å. All local patterns observed on the *C*-terrace and *R* terrace can be mapped to the model terminations, the *C*(lear) termination and the *R*(ing)

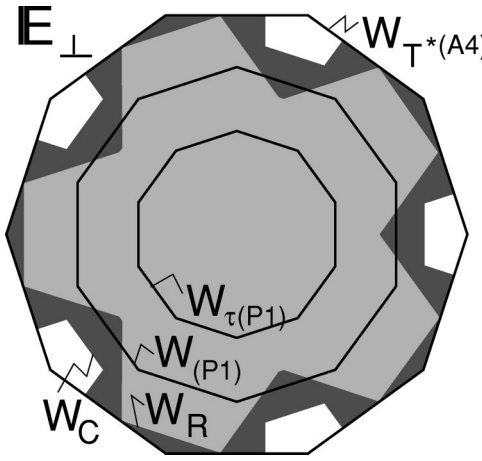

FIG. 12. In $\mathbb{E}_\perp$ the windows of the top (*q*) planes in *R* and *C* terminations, W_R and W_C, respectively. Over them is plotted (i) the window of the tiling P1 of edge length 4.8 Å (in $\mathbb{E}_\parallel$) denoted by $W_{(P1)}$. It is the maximal window of P1, such that $W_{(P1)} \subset W_C$, and (ii) the window of the tiling $\tau(P1)$, of edge length 7.8 Å (in $\mathbb{E}_\parallel$), denoted by $W_{\tau(P1)}$. It is the maximal window of P1, such that $W_{\tau P1} \subset W_R (\subset W_C)$. The scale for the figure is set by the decagon $W_{\mathcal{T}^{*(A_4)}}$, which is the window of the tiling $\mathcal{T}^{*(A_4)}$ with edges $d = \tau^{-1} D$ and $D = 4.8$ Å (in $\mathbb{E}_\parallel$). For the biggest possible window of P1 in $W_{\mathcal{T}^{*(A_4)}}$ see Fig. 5(a) in Sec. II B.

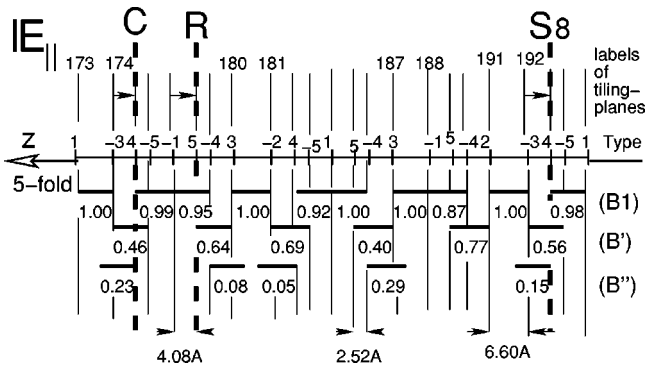

FIG. 13. A decorated Fibonacci sequence ($s=2.52$ Å, $m=4.08$ Å, $l=6.60$ Å) of the q planes along the $z_{\parallel}$ (fivefold axes) of types $\pm1,\pm2,\pm3,\pm4,\pm5$ in $\mathcal{M}$ on the *old* positions; see Ref. 19. Relative to these positions the stacked layers of the Bergman polytopes are drawn with their relative densities. The representative planes of the large *R*, *C*, and S8 terraces are marked on the *new* positions. The -4.08 Å shift from the *old* to the *new* positions is indicated by arrows.

termination, respectively; see Figs. 10(b) and 11(b). These patterns are mapped to the local atomic configurations on model terminations that contain groups of atoms in the shape of pentagons related to Bergman polytopes that are (i) either *dissected* by the termination (cB) (some of them are in the central parts of dS), or (ii) are *below* the termination (Bb) (some of them are in dS, wF, R, wSd), or (iii) to the Bergman

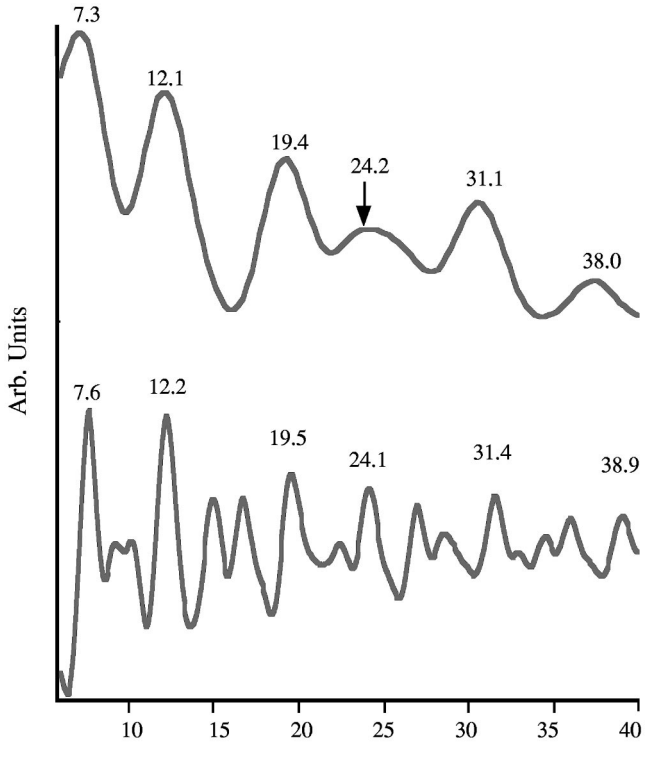

FIG. 14. Radial distributions calculated (top) from the autocorrelation pattern of the high-resolution STM image shown on Fig. 8(d); (bottom) from the autocorrelation pattern of the q plane (q-1024) of the *C* termination in the geometric model $\mathcal{M}$ presented in Fig. 10(b).

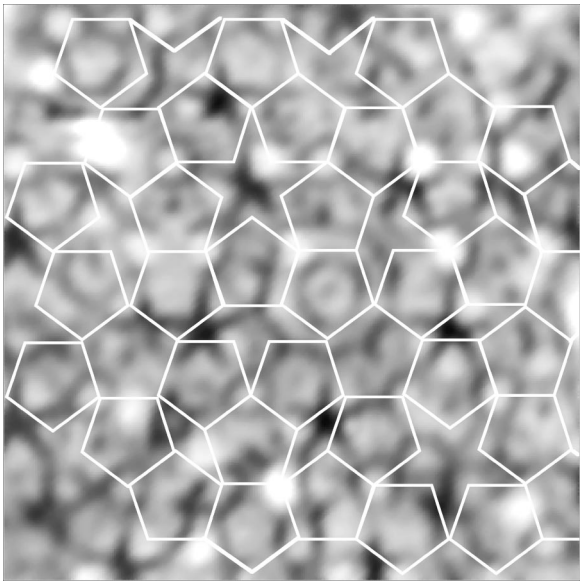

FIG. 15. 75 Å$\times$75 Å segment of an STM image of the *R* terrace with a superimposed exact patch of the P1 tiling of edge length 7.8 Å.

polytopes that are *above* the termination (Ba) (in wSu). For this see Figs. 10(b), 11(b), and 13.

B. Tiling P1 on fivefold surfaces

In order to extract information from the STM images, we have employed a tiling approach in Refs. 8 and 26. In Ref. 26 this consisted of connecting points of high contrast on the STM image to create pentagons. The filling-in of the image using pentagons led to a Penrose- (P1-) like tiling of the experimental plane (with an edge length of 7.8 Å). Here we will reconstruct exact patches of the P1 tiling on the STM images of both *R* and *C* terraces (see Figs. 15 and 16) and on corresponding model planes (not shown).

The coding regions of P1 tilings with minimal edge lengths on q planes are marked in Fig. 7. The tiling P1 with edge length 7.8 Å is coded in the interval $z_{\perp}\in(-\tau^{-1},\tau^{-1})\times[\tau^2⑤]$ and that with edge length 4.8 Å in the interval $z_{\perp}\in(-\tau^{-3},\tau^{-3})[\tau^2⑤]$.

From the coding of the q planes of the *C*, S8, and *R* terminations ($z_{\perp}^{C}=0.192\tau^2⑤$, $z_{\perp}^{S8}=0.211\tau^2⑤$, and $z_{\perp}^{R}=0.323\tau^2⑤$) we conclude that the q-1024 plane (No. 175 in Fig. 13) of the *C* termination and the q-1128 plane (No. 193 in Fig. 13) of the S8 termination in $\mathcal{M}$ allow a P1 tiling of minimal edge length 4.8 Å, and the q-1037 plane (No. 178 in Fig. 13) of the *R* termination allows a P1 tiling of minimal edge length 7.8 Å. (See also in Fig. 12 the coding windows of P1 tilings with edge lengths 4.8 and 7.8 Å plotted over the coding windows of the q-1024 plane of the *C* termination and the q-1037 plane of the *R* termination.)

An exact patch of the tiling P1 can be exactly placed on the q plane of a model termination as follows: (i) Plot the window of the P1 tiling, W_{P1}, of the maximal possible size such that $W_{P1}\subseteq W_{q\text{-}pl}$, where $W_{q\text{-}pl}$ is the coding window of the surface q plane in the model $\mathcal{M}$. For the biggest possible

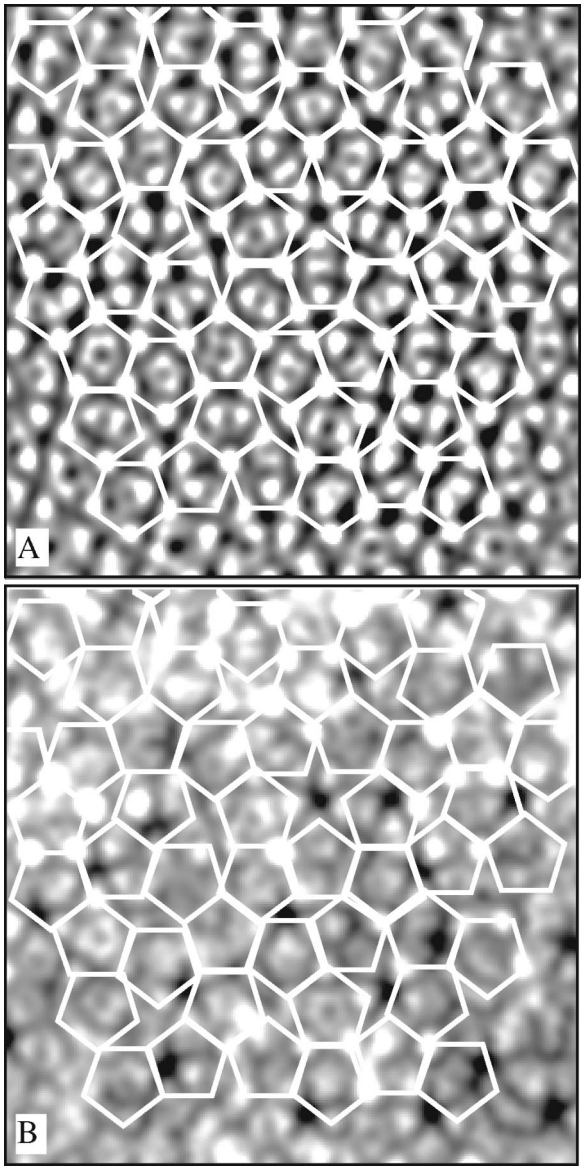

FIG. 16. (a) An exact patch of the P1 tiling superimposed on the enhanced high-resolution STM image (100 Å×100 Å) of the *C* terrace. (b) The patch of P1 tiling obtained from (a) shown superimposed on the unenhanced high-resolution STM image of the *C* termination from Fig. 8(d).

window of P1 in $W_{\mathcal{T}*(A_4)}$ see Fig. 5(a) in Sec. II B. (ii) Mark all atomic positions coded by the points in the window W_{P1} in $\mathbb{E}_{\|}$. This set of points uniquely determines the P1 tiling on the model *q* plane. The procedure is evident. In contrast, for an STM image of a terrace we have to proceed locally. If the plane is very clear and the window W_{P1} can be tightly placed in the corresponding window $W_{q\text{-}pl}$, we can reconstruct an exact patch of the P1 tiling by trial and error. A probable exact patch of the tiling P1 with minimal edge length of 7.8 Å is reconstructed on an STM image of the *R* terrace, in Fig. 15.

The *q*-1024 plane related to the surface of the *C* termination is very dense, and although we could theoretically place the P1 tiling of minimal edge length 4.8 Å (see Fig. 12), we have managed to reconstruct only an exact patch of P1 tiling of edge length 7.8 Å on the STM image of the *C* terrace; see Fig. 16. For this purpose we apply an image enhancement technique to the data of Fig. 8(d) in order to even out experimental contrast variations (inherent in the use of the STM technique which measures electron charge density at the surface rather than nuclear coordinates) and to reduce experimental noise. The procedure is based on Fourier filtering and consists of taking a fast Fourier transform of the image, and then enhancing obvious Bragg reflections with unique *k* values and removing experimentally induced diffuse features due to noise. This modified frequency space representation is then Fourier transformed to obtain the filtered image shown in Fig. 16(a). The result of this procedure is to strongly enhance features in the image corresponding to the selected *k* values. The procedure is essentially identical to that used by Soltmann and Beeli in the enhancement of high-resolution transmission electron microscopy (HRTEM) images.[45]

In the enhanced image the white spots that we interpret as the images of atomic positions are almost as sharp as in the model plane *q*-1024 from the *C* termination; see Fig. 10(b). We find a patch of exact P1 tiling of edge length 7.8 ±0.2 Å that can be easily superimposed on the enhanced image; see Fig. 16(a). Figure 16(b) shows this tiling superimposed on the unenhanced STM image.

TABLE II. Densities on *old* and *new* positions of the *R*, S8, and *C* terminations (shifted by −4.08 Å). Following Gierer *et al.* (Ref. 14) *termination* contains two planes on the surface, and in $\mathcal{M}$ its density is $\rho_{(q+b)}=\rho_{(q)}+\rho_{(b)}$; see Sec. II D.

Termination	*R*	S8	*C*	Average
No. (Pl_q^{old})	177	192	174	
$z_\perp[\tau^2⑤]$	−0.019	−0.131	−0.150	
$\rho_{(q)}^{old}$ [Å^{-2}]	0.087	0.084	0.082	
$\rho_{(b)}^{old}$ [Å^{-2}]	0.026	0.008	0.007	
$\rho_{(q+b)}^{old}$ [Å^{-2}]	0.113	0.092	0.089	0.098
No. (Pl_q^{new})	178	193	175	
$z_\perp[\tau^2⑤]$	0.323	0.211	0.192	
$\rho_{(q)}^{new}$ [Å^{-2}]	0.059	0.073	0.076	
$\rho_{(b)}^{new}$ [Å^{-2}]	0.076	0.063	0.060	
$\rho_{(q+b)}^{new}$ [Å^{-2}]	0.135	0.136	0.136	0.136

C. Densities of fivefold planes and terminations

In Table II we compare the densities of the *R*, *C*, and S8 terminations and also the densities of single (*q* and *b*) planes contained in each termination on the old and new positions. It is evident that the densities of terminations on the *new* positions give a better fit to the LEED result of Gierer *et al.*,[14] an average density of 0.136 atoms per Å^2. We see that the *C* and S8 terminations contain top *q* planes that are much more dense compared to the top *q* plane of the *R* termination. The STM images of the *C* and S8 terminations show that they are continuously clear. Another fact is that the top *q* plane of both (*C* and S8) terminations are on similar relative

positions in the bulk with respect to the layers of Bergman polytopes (compare Fig. 13): a dense layer ($B1$) is below the plane, a middle dense layer (B') is dissected by the plane, and a layer of low density (B'') is above the plane.

V. CONCLUSIONS

We have presented two atomically resolved, high-resolution STM images of large and flat terraces on the fivefold $Al_{70}Pd_{21}Mn_9$ surface. We have mapped these surfaces onto the fivefold terminations in the geometric model $\mathcal{M}$ such that they form a decorated Fibonacci sequence, and their average atomic density is in agreement with the LEED measurements of Gierer *et al.*[14] Due to the polytopal windows of the geometric model $\mathcal{M}$, *all* terminations turn out to have *equal* and simultaneously *maximal* densities. These new terminations in $\mathcal{M}$ are placed 4.08 Å lower than in the work of Ref. 19. In the present STM images the dark pentagons appear as the dark stars. At the new positions of the model-termination planes the patterns of dark pentagonal holes are the same as in Ref. 19 but now each dark hole is of an appropriate size. At the new positions the surface terminations dissect the most dense Bergman layers in the model $\mathcal{M}$. The local patterns in STM images are present in the model terminations and are related to the Bergman layers above (if one exists), below and dissected by the termination. Dissected Bergman polytopes correspond to the dark stars. The edge lengths of superimposed exact patches of the Penrose P1 tiling on two STM images (corresponding to pentagons of height equal to 12 ± 0.36 Å) are shown to be in agreement with the bulk model $\mathcal{M}$ based on the tiling $\tau\mathcal{T}^{*(2F)}$.[19]

Note added. Since this manuscript was submitted for publication, another paper containing STM results has been published; see Ref. 46. We note that those authors also conclude that the *i*-Al-Pd-Mn surface is a termination of the bulk structure.

ACKNOWLEDGMENTS

We acknowledge M. Boudard for putting his model at our disposal; the first investigations of our STM images and comparison to a bulk model were done on the fivefold planes of that model. We also acknowledge G. Booch for releasing his software components in Ada (Ref. 47) under a modified GPL. The code for handling the polyhedral windows of the geometric model $\mathcal{M}$ is based partly on these components. The EPSRC (Grant Nos. GR/N18680 and GR/N25718), NSF (Grant No. DMR-9819977), DFG (Grant No. KA 1001/4-2), and AAT (Grant No. III273-664A188816) are acknowledged for funding. We also acknowledge the University of St. Andrews for financial support.

*Corresponding author. FAX: +49 7071 29 5604. Electronic address: zorka.papadopolos@uni-tuebingen.de

[1] A. R. Kortan, R. S. Becker, P. A. Thiel, and H. S. Chen, Phys. Rev. Lett. **64**, 200 (1990).
[2] T. M. Schaub, D. E. Bürgler, H.-J. Güntherodt, and J.-B. Suck, Phys. Rev. Lett. **73**, 1255 (1994).
[3] T. M. Schaub, D. E. Bürgler, C. Schmidt, H.-J. Güntherodt, and J.-B. Suck, Z. Phys. B: Condens. Matter **96**, 93 (1994).
[4] T. M. Schaub, D. E. Bürgler, H.-J. Güntherodt, J.-B. Suck, and M. Audier, Appl. Phys. A: Mater. Sci. Process. **61**, 491 (1995).
[5] T. M. Schaub, D. E. Bürgler, C. Schmidt, and H.-J. Güntherodt, J. Non-Cryst. Solids **205/207**, 748 (1996).
[6] Ph. Ebert, F. Yue, and K. Urban, Phys. Rev. B **57**, 2821 (1998).
[7] Z. Shen, C. R. Stoldt, C. J. Jenks, T. A. Lograsso, and P. A. Thiel, Phys. Rev. B **60**, 14 688 (1999).
[8] J. Ledieu, A. Munz, T. Parker, R. McGrath, R. D. Diehl, D. W. Delaney, and T. A. Lograsso, Surf. Sci. **433/435**, 665 (1999).
[9] J. Ledieu, A. Munz, T. Parker, R. McGrath, R. D. Diehl, D. W. Delaney, and T. A. Lograsso, in *Quasicrystals*, edited by J. M. Dubois, P. A. Thiel, A. P. Tsai, and K. Urban, MRS Symposia Proceedings No. 553 (Materials Research Society, Warrendale, PA, 1999), p. 237.
[10] D. Naumović, P. Aebi, L. Schlapbach, and C. Beeli, in *New Horizons in Quasicrystals: Research and Applications*, edited by A. I. Goldman, D. J. Sordelet, P. A. Thiel, and J. M. Dubois (World Scientific, Singapore, 1997).
[11] D. Naumović, P. Aebi, L. Schlapbach, C. Beeli, T. A. Lograsso, and D. W. Delaney, in *Proceedings of the 6th International on Quasicrystals (ICQ-6, Yamada Conference XLVII)*, edited by S. Takeuchi and T. Fujiwara (World Scientific, Singapore, 1998).
[12] D. Naumović, P. Aebi, C. Beeli, and L. Schlapbach, Surf. Sci. **433-435**, 302 (1999).
[13] M. Gierer, M. A. Van Hove, A. I. Goldman, Z. Shen, S.-L. Chang, C. J. Jenks, C.-M. Zhang, and P. A. Thiel, Phys. Rev. Lett. **78**, 467 (1997).
[14] M. Gierer, M. A. Van Hove, A. I. Goldman, Z. Shen, S.-L. Chang, P. J. Pinhero, C. J. Jenks, J. W. Anderegg, C.-M. Zhang, and P. A. Thiel, Phys. Rev. B **57**, 7628 (1998).
[15] M. Boudard, M. de Boissieu, C. Janot, G. Heger, C. Beeli, H.-U. Nissen, H. Vincent, R. Ibberson, M. Audier, and J. M. Dubois, J. Phys.: Condens. Matter **4**, 10 149 (1992).
[16] V. Elser, Philos. Mag. B **73**, 641 (1996).
[17] P. Kramer, Z. Papadopolos, and W. Liebermeister, in *Proceedings of the 6th International Conference on Quasicrystals, Yamada Conference XLVII*, edited by S. Takeuchi and T. Fujiwara (World Scientific, Singapore, 1998), p. 71.
[18] Z. Papadopolos, P. Kramer, and W. Liebermeister, in *Proceedings of the International Conference on Aperiodic Crystals, Aperiodic 1997*, edited by Marc de Boissieu, Jean-Louis Verger-Gaugry, and Roland Currant (World Scientific, Singapore, 1998), p. 173.
[19] G. Kasner, Z. Papadopolos, P. Kramer, and D. E. Bürgler, Phys. Rev. B **60**, 3899 (1999).
[20] Z. Papadopolos, P. Kramer, G. Kasner, and D. Bürgler, in *Quasicrystals* (Ref. 9), p. 231.
[21] P. Kramer, Z. Papadopolos, and H. Teuscher, J. Phys.: Condens. Matter **11**, 2729 (1999).
[22] D. S. Rokhsar, N. D. Mermin, and D. C. Wright, Phys. Rev. B **35**, 5487 (1987).
[23] P. Kramer, Z. Papadopolos, and D. Zeidler, in *Symmetries in Science V: Algebraic Structures, Their Representations, Realizations and Physical Applications*, edited by B. Gruber and L. C. Biedenharn (Plenum, New York, 1991), p. 395.

[24] A. Katz and D. Gratias, in *Proceedings of the 5th International Conference on Quasicrystals*, edited by C. Janot and R. Mosseri (World Scientific, Singapore, 1995), p. 164.

[25] The Bergman polytope is a dodecahedron with particular concave pentagonal faces; see Ref. 16.

[26] J. Ledieu, R. McGrath, R. D. Diehl, T. A. Lograsso, D. W. Delaney, Z. Papadopolos, and G. Kasner, Surf. Sci. **492/3**, L729 (2001).

[27] The diffraction peaks of an F phase are labeled by six (half-integer) coordinates, the points in D_6^{rec}. The six-dimensional lattice D_6^{rec} is reciprocal to the root lattice D_6. For the points in D_6^{rec} see Table I in Sec. II C.

[28] A point $q \in D_6$ is presented by six integers $(n_1, \ldots, n_6)$, such that $\Sigma_{i=1}^{6} n_i =$ even.

[29] J. H. Conway and N. J. A. Sloane, *Sphere Packings, Lattices and Groups* (Springer, New York, 1988).

[30] M. de Boissieu, P. Stephens, M. Boudard, C. Janot, D. L. Chapman, and M. Audier, J. Phys.: Condens. Matter **6**, 10 725 (1994).

[31] M. Baake, P. Kramer, M. Schlottmann, and D. Zeidler, Int. J. Mod. Phys. B **4**, 2217 (1990).

[32] Z. Papadopolos, C. Hohneker, and P. Kramer, Discrete Math. **221**, 101 (2000).

[33] These prototiles can be uniquely reconstructed from the point set of atomic positions.

[34] K. Edagawa, K. Suzuki, and S. Takeuchi, Phys. Rev. Lett. **85**, 1674 (2000).

[35] P. Kramer, J. Phys. A **32**, 5781 (1999).

[36] P. Kramer, Mater. Sci. Eng., A **294-296**, 401 (2000).

[37] Z. Papadopolos and G. Kasner, in *Coverings of Discrete Quasiperiodic Sets, Theory and Applications to Quasicrystals*, edited by P. Kramer and Z. Papadopolos, Springer Tracts in Modern Physics, Vol. 180 (Springer, Berlin, 2002), p. 165.

[38] B. Grünbaum and G. C. Shepard, *Tilings and Patterns* (Freeman, San Francisco, 1987).

[39] K. Niizeki, J. Phys. A **22**, 4281 (1989).

[40] Z. Papadopolos and P. Kramer, in *Proceedings of Aperiodic '94*, edited by G. Chapuis and W. Paciorek (World Scientific, Singapore, 1995), pp. 70–76.

[41] R. V. Moody, in *The Mathematics of Long-Range Aperiodic Order*, edited by R. V. Moody (Kluwer, Dordrecht, 1997), p. 403.

[42] D. W. Delaney, T. E. Bloomer, and T. A. Lograsso, in *New Horizons in Quasicrystals: Research and Applications*, edited by A. I. Goldman, D. J. Sordelet, P. A. Thiel, and J. M. Dubois (World Scientific, Singapore, 1997).

[43] C. Jenks, D. W. Delaney, T. E. Bloomer, S.-L. Chang, T. A. Lograsso, Z. Shen, C.-M. Zhang, and P. A. Thiel, Appl. Surf. Sci. **103**, 485 (1996).

[44] M. Kishida, Y. Kamimura, R. Tamura, K. Edagawa, S. Takeuchi, T. Sato, Y. Yokoyama, J. Q. Guo, and A. P. Tsai, Phys. Rev. B **65**, 094208 (2002).

[45] C. Soltmann and C. Beeli, Philos. Mag. Lett. **81**, 877 (2001).

[46] L. Barbier, D. Le Floc'h, Y. Calvayrac, and D. Gratias, Phys. Rev. Lett. **88**, 085506 (2002).

[47] G. Booch, *Software Components with Ada, Structures, Tools, and Subsystems* (Benjamin-Cummings, New York, 1991).